ACS OMEGA

http://pubs.acs.org/journal/acsodf

Article

Investigation on the Promoter-Induced Rapid Non-Aqueous Media Synthesis of SAPO-35 and Methanol-to-Olefin Reaction

Suresh Siliveri, Sai Siva Kumar Pinnepalli, Deepak Joshi, Suman Chirra, Srinath Goskula, Sripal Reddy Gujjula, Nathan A. Oyler, and Venkatathri Narayanan*

Cite This: *ACS Omega* 2021, 6, 5661−5669

Read Online

ACCESS | Metrics & More | Article Recommendations

ABSTRACT: Microporous SAPO-35 molecular sieves (Levyne type) were synthesized in non-aqueous media by using different inorganic promoters ($HClO_4^-$, HF, H_3PO_4, and $NaNO_3$) to enhance the rate of crystallization, and the as-synthesized materials were characterized by using different methods such as powder X-ray diffraction spectroscopy (PXRD), scanning electron microscopy (SEM), Fourier transform infrared spectroscopy (FT-IR), magic angle spinning-nuclear magnetic resonance spectroscopy (MAS-NMR), Brunauer−Emmett−Teller (BET) analysis, and X-ray photoelectron spectroscopy (XPS). From PXRD patterns, it was found that all the materials have a highly crystalline nature without any other impurities. SEM images reveal rhombohedral particles in all synthesis conditions. The framework structure of the synthesized materials was identified by FT-IR spectroscopy, and it reveals that all materials gave a similar framework structure. From BET and XPS, we have confirmed that the pore size and pore diameters along with the elemental compositions have a minor change. The ^{27}Al, ^{31}P, and ^{29}Si MAS-NMR spectra of all the promoter-based SAPO-35 materials are close to those of the standard SAPO-35 material. All the above characterization studies reveal the formation of SAPO-35 in a short time with promoters. The catalytic application studies of these synthesized materials for a methanol-to-olefin conversion reaction were performed, and the efficiency of these materials was found to be similar to that of standard materials.

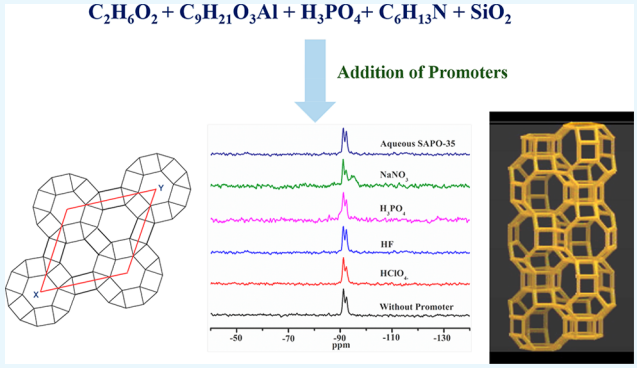

1. INTRODUCTION

Molecular sieves AlPOs and SAPOs are ordered porous materials, they were synthesized three decades ago,[1−3] and their basic structural framework resembles certain zeolite materials, for example, SAPO-35 (Levyne structure).[4,5] Contrarily, there are several other AlPOs and SAPOs reported in the literature whose structural framework does not resemble any zeolite material. Basically, the AlPOs are neutral in nature, and hence they provide no catalytic activity.[6] However, introducing silicon into the AlPO framework makes them acidic (SAPO) and hence catalytic activity can be attained.[7,8] These SAPOs possess certain unique catalytic properties,[9] for instance, adsorption,[10] separation,[11] and ion-exchange.[12] Moreover, these materials are highly stable thermally and chemically. There are at least two hundred different topologies of these molecular sieves that have been reported in the literature so far, and more studies are being carried out currently across the globe.[13,14] By virtue of their unique properties, these materials have received considerable attention from researchers around the world.

Conventional synthesis of molecular sieves mainly involves trial and error of variation in synthesis parameters. However, the necessity for the synthesis of molecular sieves with the desired structural framework and properties has created the need to develop new synthesis methods. These synthesis methods were constructed mainly on the understanding of the mechanism of a crystallization process. The new synthesis methods are hydrothermal, solvo-thermal, microwave-assisted, sol−gel, etc.[15,16] Among all these methods available, the hydrothermal method is the most convenient process of synthesizing the molecular sieves with desired morphological framework structures. This can be achieved due to the higher temperatures and autogenous pressure involved in the synthesis process.

Although the hydrothermal method is accurate in achieving the desired morphological frameworks, the crystallization time is very long. This makes it less feasible in the commercial

Received: December 15, 2020
Accepted: February 11, 2021
Published: February 19, 2021

https://dx.doi.org/10.1021/acsomega.0c06109
ACS Omega 2021, 6, 5661−5669

synthesis of SAPOs. This limitation in the hydrothermal method can be overcome by using different types of promoters,[17] for example, $HClO_4^-$ and H_3PO_4.

SAPO-35 is a LEV (Levyne)-type topological framework microporous material with 0.36 × 0.48 nm ring opening pores, which are constructed by a single six-membered ring (S6R) and a double six-membered ring (D6R) with different T-sites in a 2:1 ratio, respectively.[18] It was synthesized using quinuclidine, cyclohexylamine, and hexamethyleneimine as the structure-directing agents (SDAs) for the crystallization of SAPO-35 at a 200 °C reaction temperature in aqueous media.[4,19] A very recent study revealed that SAPO-35 molecular sieves have been synthesized in a non-aqueous medium (ethylene glycol) using hexamethyleneimine as an SDA at 200 °C for a crystallization time of about 360 h.[20] This non-aqueous media samples showed a better crystalline nature as compared to the aqueous samples. The only drawback was that it consumed more time.

The MTO (methanol-to-olefin) reaction is one of the most important reactions for the production of petrochemicals.[21−24] The catalytic conversion of MTO is one of the promising ways of converting natural gas and coal to chemicals. This MTO reaction was first proposed by Mobil Corporation in 1977. The methanol-to-olefin reaction is an acid-catalyzed reaction. Researchers widely studied this MTO reaction with different zeolites; Si was incorporated to molecular sieves, and from these studies, it was found that SAPO-34, SAPO-35, and HZSM-5 are better catalysts for the conversion of methanol to olefins.[23,25,26]

Hence, in the present study, we have demonstrated the synthesis of SAPO-35 microporous molecular sieves in a non-aqueous medium through the conventional hydrothermal process by adding small amounts of inorganic promoters, namely, $HClO_4^-$, HF, H_3PO_4, and $NaNO_3$, in order to enhance the crystallization process such that the crystallization time is reduced. The as-synthesized SAPO-35 molecular sieves from the above method were used as catalysts in the MTO reaction as an application study. Moreover, we also have compared the MTO activity of the conventional SAPO-35 sample at 360 h with promoter-based SAPO-35 samples.

2. RESULTS AND DISCUSSION

2.1. PXRD Analysis. All the synthesized samples were analyzed using the PXRD technique to identify the nature of crystallinity. Figure 1 represents the PXRD patterns of the SAPO and promoter samples, and it can be observed from Figure 1 that the peaks at 2θ values of 10.9, 13.3, 17.3, 21.9, 26.6, and 32.3° correspond to Miller indices of (012), (110), (104), (024), (220), and (134) planes, respectively. As per the literature [JCPDS: 51−0052], it is confirmed that the synthesized SAPO-35 has a Levyne-type hexagonal crystalline structure.[18,27] Furthermore, the relative crystallinity of each sample was calculated using the most prominent peak in the corresponding PXRD pattern, which was observed at a 2θ value of 21.9° corresponding to the (024) plane. In order to calculate the relative crystallinity of the synthesized samples, the relative crystallinity of the standard sample prepared at 360 h was taken as 100%. The equation used for the calculation of relative crystallinity is given below:

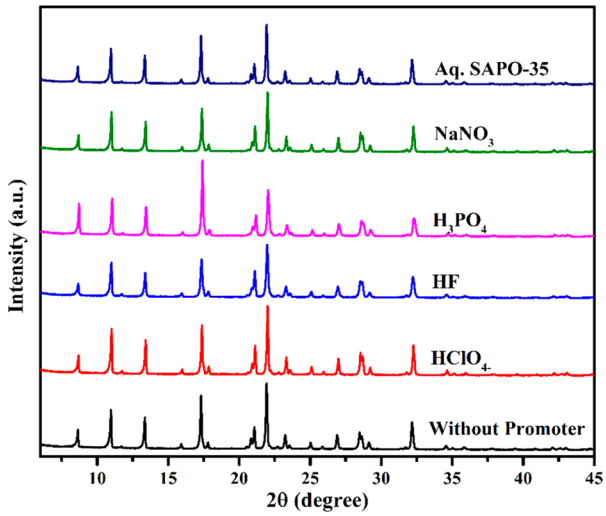

Figure 1. PXRD patterns of standard SAPO-35, SAPO-35 with $HClO_4^-$ as the promoter, HF as the promoter, H_3PO_4 as the promoter, and $NaNO_3$ as the promoter, and aqueous media SAPO-35.

$$\text{relative crystallinity} = \frac{\text{area under the curve (024) plane of particular sample}}{\text{area under the curve (024) plane of the standard sample}} \times 100 \quad (1)$$

The average crystallite size of all the synthesized samples was calculated using eq 2, and the results are tabulated in Table 1:

$$\text{crystallite size} = \frac{K\lambda}{\beta \cos\theta} \quad (2)$$

Table 1. Relative Crystallinity and Average Crystallite Size of the Synthesized Materials

S. no.	sample	relative crystallinity (%)	avg. crystallite size (nm)
1	without promoter	100	68
2	$HClO_4^-$	99.76	71
3	HF	93.49	59
4	H_3PO_4	83.67	50
5	$NaNO_3$	77.4	47
6	aq. SAPO-35	89.96	68

where K is the dimensionless shape factor (0.9), λ is the X-ray wavelength (1.5418 Å), β is the line broadening at half the maximum intensity at the 2θ angle, and θ is the Bragg angle.

The relative crystallinity of materials synthesized in the presence of $HClO_4^-$ and HF as promoters has shown similarity with that of the standard sample. This indicates that in the presence of both the promoters, the crystallinity is considerably good. However, in the case of materials synthesized in the presence of H_3PO_4 and $NaNO_3$ as promoters, the relative crystallinity is slightly less but considerably in a good amount. This reduction in relative crystallinity may be because of the slower rate of crystallization in SAPO-35 having H_3PO_4 and $NaNO_3$ as promoters compared to SAPO-35 having $HClO_4^-$ and HF as promoters. The average crystallite size of synthesized SAPO-35 without promoter in non-aqueous medium and aqueous medium was found to be 68 nm. This value has increased to 71 nm for the synthesized SAPO-35 in the presence of $HClO_4^-$ promoter. The average crystallite size

https://dx.doi.org/10.1021/acsomega.0c06109
ACS Omega 2021, 6, 5661−5669

of the remaining synthesized SAPO-35 material with other promoters was found to be in a range of 47−59 nm.

2.2. SEM Analysis. The morphology of all synthesized SAPO-35 materials was observed by SEM. The SEM images, as shown in Figure 2, revealed that all the samples are highly

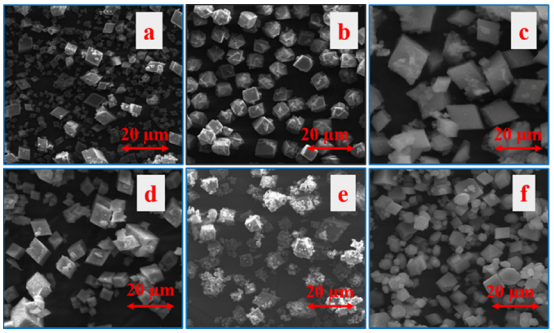

Figure 2. SEM images of SAPO-35 (a) Standard Non-Aqueous 360 h, (b) $HClO_4^-$ as the promoter, (c) HF as the promoter, (d) H_3PO_4 as the promoter, (e) $NaNO_3$ as the promoter, and (f) aqueous media 48 h.

crystalline in nature without any amorphous phase material except in the case of SAPO-35 synthesized using $NaNO_3$ as a promoter. When $NaNO_3$ was used as a promoter, even though the nucleation process in the reaction has occurred rapidly, the consequent crystallization process might not have happened completely. Therefore, as a result, less crystallinity was observed in the $NaNO_3$ promoter case. These SEM results are in good agreement with PXRD results as there is crystallinity in the synthesized materials. From SEM images, it can be seen that the structure of the crystals is rhombohedral and the size of the crystals was uniform throughout.

2.3. FT-IR Analysis. FT-IR studies were carried out to identify the framework configuration of all SAPO-35 samples. The corresponding FT-IR spectra are illustrated in Figure 3. From these spectra, we could infer that the peaks that appeared at wavenumbers 500 and 645 cm^{-1} correspond to T−O−T (where T = Si, Al, and P) symmetric stretching frequency and

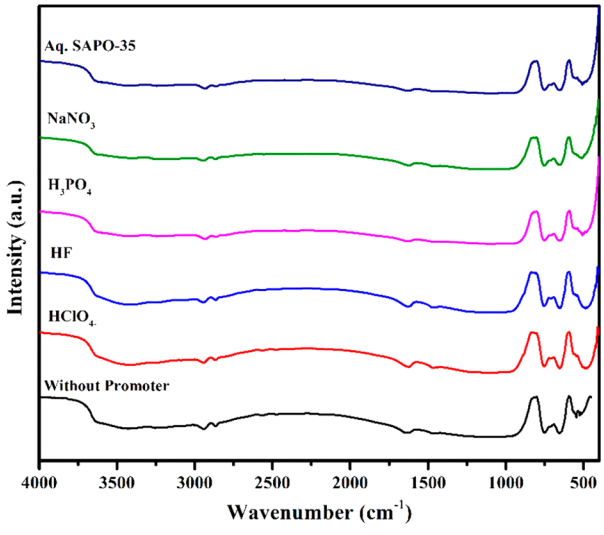

Figure 3. FT-IR spectra of standard SAPO-35, SAPO-35 with $HClO_4^-$ as the promoter, HF as the promoter, H_3PO_4 as the promoter, and $NaNO_3$ as the promoter, and aqueous media SAPO-35.

protonated template, respectively. Meanwhile, the peak that appeared at 750 cm^{-1} is due to T−O bending in the double six-membered ring (D6R) and T−O bending of the Si tetrahedral structure. Moreover, the peak that appeared in the range 2600−3000 cm^{-1} is a consequence of the stretching frequency of −CH, resulting from the organic environment like templates, organic functional silane, etc. The stretching vibrations around 1600 and 1400 cm^{-1} could be ascribed to physically adsorbed water molecules from atmospheric air (i.e., H−O−H bending mode). Based on the FT-IR results, it appears that the framework structures of the SAPO-35 materials synthesized using promoters and without using promoters are the same.

2.4. MAS-NMR Studies. To identify the local environment in the structural framework of the synthesized SAPO-35 materials, ^{27}Al, ^{29}Si, and ^{31}P MAS-NMR spectroscopic studies[28,29] were carried out.

The ^{27}Al MAS-NMR spectra of SAPO-35 in all cases are depicted in Figure 4. The spectrum in the case of synthesized

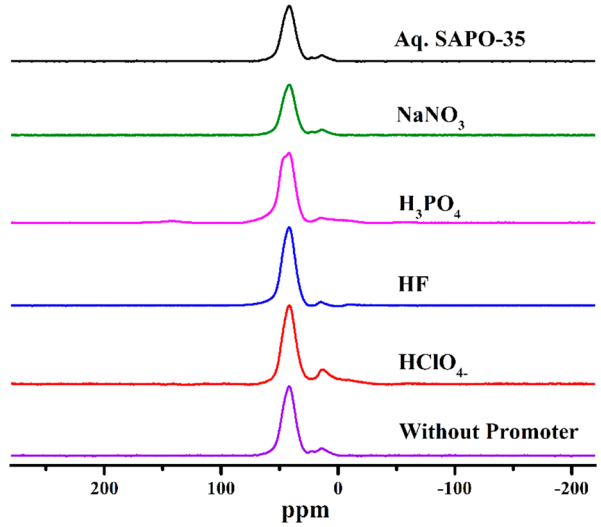

Figure 4. ^{27}Al MAS-NMR spectra of standard SAPO-35, SAPO-35 with $HClO_4^-$ as the promoter, HF as the promoter, H_3PO_4 as the promoter, and $NaNO_3$ as the promoter, and aqueous media SAPO-35.

SAPO-35 without a promoter at 360 h exhibits two peaks at 41.98 ppm (strong) and 13.97 ppm (weak). The strong peak at 41.98 ppm is attributed to the tetrahedral $Al[Al(OP)_4(OH)_2]$ of the SAPO-35 framework, and the weak peak at 13.97 is due to the octahedral unreacted Al source. Similar to SAPO-35 without a promoter at 360 h, the others with various promoters also exhibit similar peaks, which indicates the formation of SAPO-35 in all the cases.

The incorporation of silicon has been confirmed by the evidence of ^{29}Si MAS-NMR spectroscopic studies. The resulting ^{29}Si MAS-NMR spectra are presented in Figure 5. From the spectrum of the synthesized SAPO-35 material without promoter at 360 h, two peaks at −87.14 ppm and −93.22 ppm can be observed. The appearance of two different peaks emphasizes the incorporation of Si in both single six-membered ring $[Si_{T1}(OAl)_4]$ and in double six-membered ring $[Si_{T1}(OAl)_4]$ frameworks.[30,31] From these results, the formation of Levyne-type SAPO-35 framework was confirmed. The remaining materials of SAPO-35 synthesized with promoters have also exhibited identical peaks to the reference

https://dx.doi.org/10.1021/acsomega.0c06109
ACS Omega 2021, 6, 5661−5669

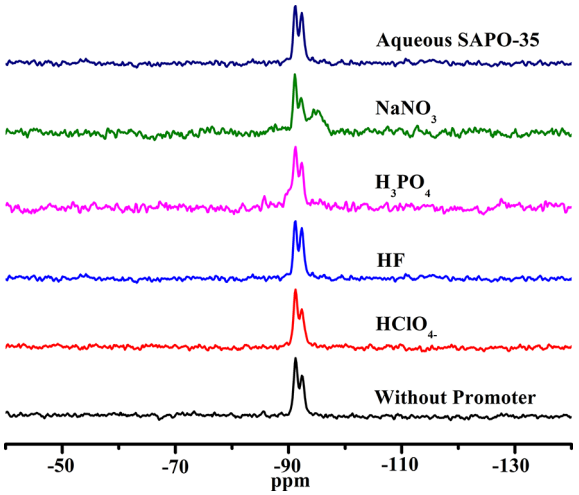

Figure 5. ^{29}Si MAS-NMR spectra of standard SAPO-35, SAPO-35 with $HClO_4^-$ as the promoter, HF as the promoter, H_3PO_4 as the promoter, and $NaNO_3$ as the promoter, and aqueous media SAPO-35.

SAPO-35 material at 360 h. This indicated the successful incorporation of silicon into the framework.

From the ^{31}P MAS-NMR spectrum (Figure 6) of the SAPO-35 material synthesized without a promoter at 360 h, we can

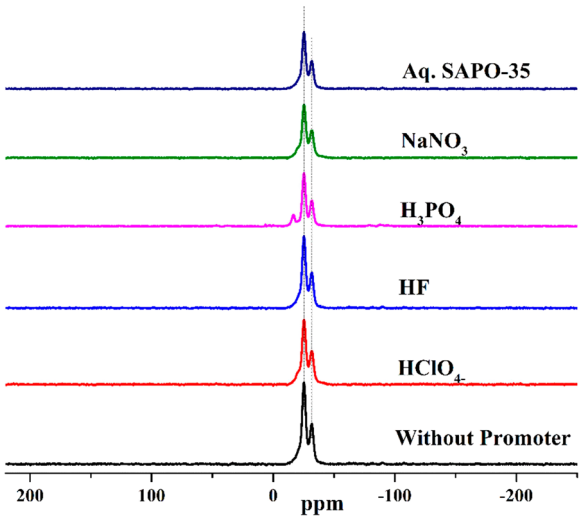

Figure 6. ^{31}P MAS-NMR spectra of standard SAPO-35, SAPO-35 with $HClO_4^-$ as the promoter, HF as the promoter, H_3PO_4 as the promoter, and $NaNO_3$ as the promoter, and aqueous media SAPO-35.

observe two peaks precisely at −25.22 ppm (strong intensity) and −31.72 ppm (weak intensity). These two peaks represent phosphorus in the form of $P(Al)_4$ as a tetrahedron coordinated with two different crystallographic T-sites.[4] The ratio of peak intensities has a value of 1.94 [$P_{T1}(-25.22)/P_{T2}(-31.72)$], which is very close to the theoretical value of 2. Furthermore, the ^{31}P MAS-NMR spectra of the SAPO-35 material synthesized using different promoters in the present study have also demonstrated results that are identical to the results of standard materials. Interestingly, the ^{31}P MAS-NMR spectrum of the SAPO-35 material in the case of H_3PO_4 as a promoter showed one narrow (weak intensity) peak at −16.67 ppm in addition to the regular peaks. This narrow peak may be because of P species in the layered phase, where these P atoms are situated in an orderly environment even after the partial condensation of P in the layered phase as observed from the chemical shift values.

Hence, from all the above ^{27}Al, ^{29}Si, and ^{31}P MAS-NMR spectra, we can emphasize that the synthesized SAPO-35 materials using promoters were identical to the SAPO-35 synthesized without a promoter at 360 h.

2.5. BET and XPS Analyses. Surface area measurement is a significant parameter in porous materials, and therefore SAPO-35 was tested by N_2 adsorption−desorption. The N_2 adsorption−desorption isotherm and the pore distribution curve of the calcined SAPO-35 molecular sieve are presented in Table 2. The BET specific surface area from the table was

Table 2. Textual Properties of SAPO-35 Materials

gel composition	surface area (m^2/g)	pore volume (cm^3/g)	pore diameter (nm)	elemental composition (mol %) XPS
sample-1 (standard)	449	0.22	1.97	$Si_{0.195}Al_{0.422}P_{0.322}$
sample-2 ($HClO_4^-$)	446	0.22	1.97	$Si_{0.189}Al_{0.461}P_{0.361}$
sample-3 (HF)	440	0.22	1.96	$Si_{0.186}Al_{0.468}P_{0.345}$
sample-4 (H_3PO_4)	446	0.22	1.98	$Si_{0.177}Al_{0.466}P_{0.329}$
sample-5 ($NaNO_3$)	461	0.23	2.01	$Si_{0.179}Al_{0.461}P_{0.361}$
sample-6 (aq. media)	444	0.22	1.97	$Si_{0.187}Al_{0.484}P_{0.326}$

found to be similar for SAPO-35 synthesized with and without promoters. In the case of standard non-aqueous SAPO-35 materials at 360 h, the surface area was 449 m^2/g with a pore volume and pore diameter of about 0.22 cm^3/g and 1.97 nm, respectively. Meanwhile, in the case of perchlorate and H_3PO_4 promoter-based SAPO-35 materials, the surface area is identical but there is a slight difference in pore volume and pore diameter. The HF promoter-based SAPO-35 material has a surface area of 440 m^2/g, pore volume of 0.22 cm^3/g, and pore diameter of 1.96 nm. Interestingly, the $NaNO_3$ promoter-based SAPO-35 material has shown the highest surface area, pore volume, and pore diameter, i.e., 461 m^2/g, 0.23 cm^3/g, and 2.01 nm, respectively. This may be due to the impure phase of SAPO-35. In all SAPO-35 materials, the isotherm shows the characteristics of microporous materials at a low relative pressure P/P_0 with a type-IV hysteresis at a high relative pressure P/P_0.

Surface elemental analysis was carried out by XPS studies. Figure 7 represents XPS core spectra of the synthesized materials and the results given in Table 2 were in accordance with the theoretical values (elemental binding energy values of respective elements), and it has been observed that the results support the MAS-NMR results, which confirmed the Si incorporation in SAPO-35 materials.

From all these above studies, it was observed that the formation of SAPO-35 in all the promoter-based materials showed similar textual properties.

2.6. Investigation of the Phase Transformation Mechanism. In general, SAPO formation occurs by reaction of the Al source with the P source, forming aluminum phosphate frameworks, which are neutral, and when the Si source is added along with the SDA, the desired SAPO products will be formed.[32−34] Here, in our case, aluminum

https://dx.doi.org/10.1021/acsomega.0c06109
ACS Omega 2021, 6, 5661−5669

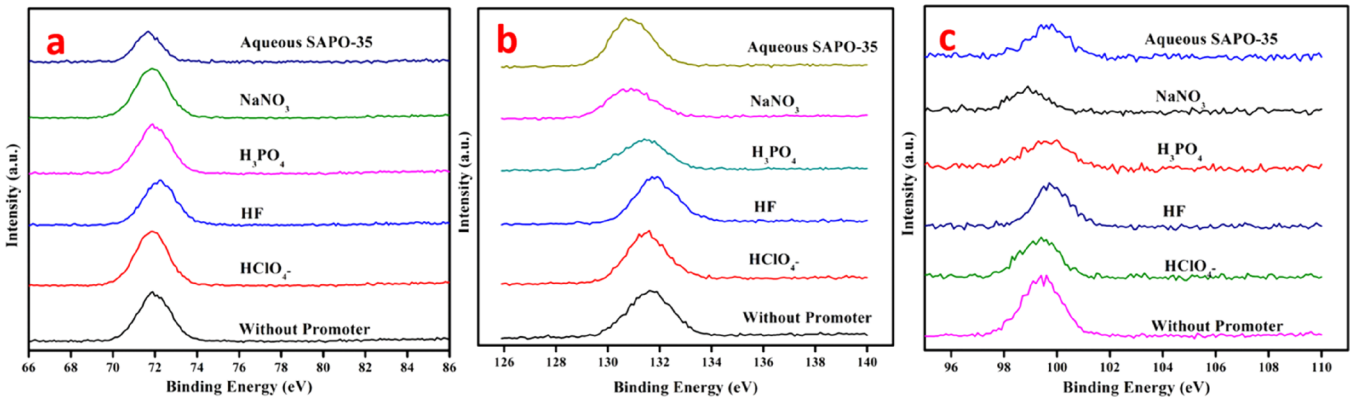

Figure 7. XPS core spectra of (a) Al, (b) P, and (c) Si.

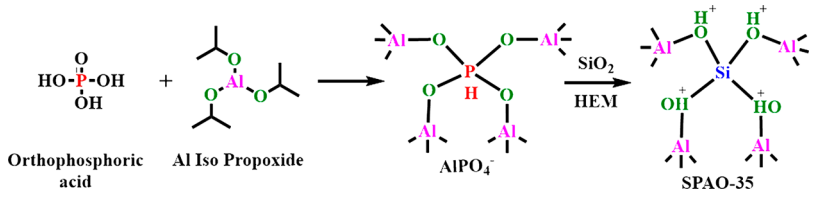

Figure 8. Schematic representation of SAPO formation.

isopropoxide also as the Al source and orthophosphoric acid as the P source in the presence of the media are condensed to form the $AlPO_4^-$ framework. After the formation of the $AlPO_4^-$ framework, by addition of SiO_2 along with HEM (SDA), replacement of Si ions with P in the $AlPO_4^-$ framework occurred, which is called Si/P exchange and is given in Figure 8. Here, when we use the promoter after the formation of the $AlPO_4^-$ framework, the Si/P exchange process will be faster. Hence, the promoters play an important role in the transformation of the $AlPO_4^-$ framework to the SAPO phase and in the fast crystallization growth.

The formation of SAPOs will take place in two steps, the first one being nucleation followed by crystal growth. In a regular approach of SAPO's preparation, the initial nucleation of the gel step takes a longer time, resulting in slower crystallization, which is the main drawback of this synthesis procedure. When a small amount of inorganic promoter is added to the reaction mixture, this enhances the speed of the nucleation process of the gel and leads to faster crystal growth.[35]

Nucleation is the preliminary process that happens in the formation of a crystal from a solution/liquid/vapor, in which a small number of ions, atoms, or molecules are arranged in a pattern characteristic of a crystalline solid, forming a site upon which additional particles are deposited as the crystal grows. Supersaturation is the driving force for crystallization nucleation and growth and will ultimately dictate the final crystal size distribution.

Figure 9 represents the crystallization kinetics of SAPO-35 in the presence of each promoter, in which the % crystallization against the reaction time is plotted. From the above plot, it can be observed that the nucleation and crystallization are very fast for the material synthesized using promoters compared to the standard sample.

An increase in the concentration of promoter decreases the crystallization time up to a saturated level, and thereafter, it remains constant (at optimum concentration). The activation energy for nucleation (E_n) was calculated from the expression

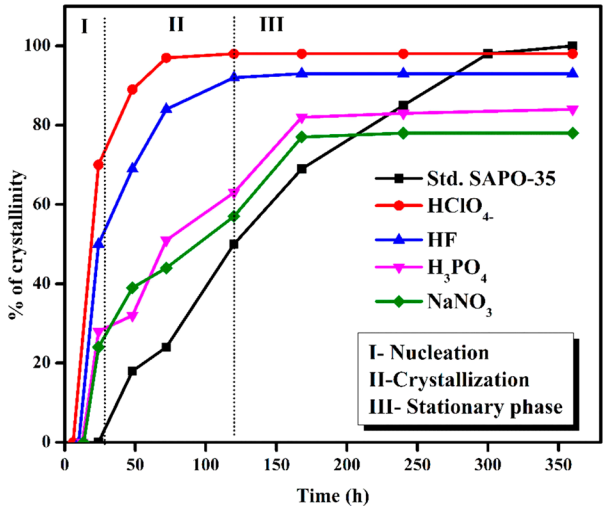

Figure 9. Crystallization kinetics of standard SAPO-35, SAPO-35 with $HClO_4^-$ as the promoter, HF as the promoter, H_3PO_4 as the promoter, and $NaNO_3$ as the promoter, and aqueous media SAPO-35.

$$\frac{d\ln\left(\frac{1}{n}\right)}{d\left(\frac{1}{T}\right)} = -E_n/R$$

where "n" is the induction period, viz., the point of the crystallization at which transformation to the crystalline phase just occurs. Correspondingly, E_c, the activation energy for crystal growth, was calculated as the rate of crystallization and was obtained from the point in the crystallization curve at which crystallization was 50%. The rate equation can be represented as

$$\frac{d\ln\left(\frac{1}{\theta}\right)}{d\left(\frac{1}{T}\right)} = -\frac{E_c}{R}$$

https://dx.doi.org/10.1021/acsomega.0c06109
ACS Omega 2021, 6, 5661−5669

where θ represents the time in hours for 50% crystallization.

From these results, the order of the nucleation and crystallization can be given as $HClO_4^-$ > HF > H_3PO_4 > $NaNO_3$ > without promoter. Interestingly, the crystallinity of promoter-based samples was less than that of the sample without a promoter, but the morphology is uniform compared to that of the standard sample. This may be due to the superior nucleation and faster crystallization rate.

2.7. Catalytic Application Study. The catalytic activity of all the synthesized SAPO-35 materials using promoters along with standard non-aqueous and aqueous SAPO-35 materials to convert methanol-to-olefins (MTO) was performed at 350 °C with a WHSV (weight hourly space velocity) of 6.5 h^{-1}. MTO conversion is a reaction in which the methanol will be converted into different types of olefins based on the catalysts used (different SAPO materials), as shown in Figure 10. The

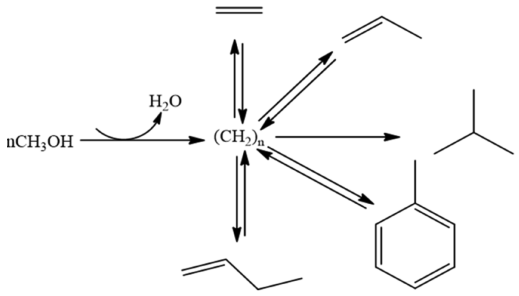

Figure 10. Schematic MTO reaction product illustrations

Table 3. Catalytic Activity of SAPO-35 Materials

S. no.	sample	selectivity (%)	conversion rate (%)	TON	TOF
1	without promoter	99	97	60.54	0.0168
2	$HClO_4^-$	97	95.6	64.78	0.0179
3	HF	94	92	64.67	0.0179
4	H_3PO_4	94	92	64.38	0.0178
5	$NaNO_3$	90	84	58.52	0.0162
6	Aq. SAPO-35	96	87	57.65	0.0160

obtained results are listed in Table 3. From these activity data, we can observe that the standard non-aqueous SAPO-35 material's conversion activity is about 97%, the major product of the reaction is 1-butene, and selectivity is over 99%. The SAPO-35 material synthesized using perchlorate as a promoter has also shown similar performance, which is about 95.6% conversion. Meanwhile, HF and H_3PO_4 promoter-based SAPO-35 materials have obtained around 92% yield, which is slightly lower compared to the standard non-aqueous SAPO-35 and perchlorate promoter-based SAPO-35 materials. This may be due to the less crystalline nature of the material, which was already discussed in the previous section. Meanwhile, the $NaNO_3$ promoter-based SAPO-35 material has given the least yield conversion and least selectivity as well. This is because of the impure phase of SAPO-35 and lower crystalline nature of the material. By comparing all the above results, it could be concluded that the non-aqueous media SAPO-35 materials are superior in crystalline nature and MTO conversion reaction performance when compared to the aqueous media SAPO-35 material. Hence, it is stated that the promoter-based non-aqueous SAPO-35 and standard non-aqueous SAPO-35 materials were able to perform efficiently in converting methanol to olefins.

We have also calculated the turnover number (TON) and turnover frequency (TOF) values using the equation in section 4.3. The turnover number value for standard SAPO-35 has been observed to be 60.54. Interestingly, the turnover number for SAPO-35 in the presence of $HClO_4^-$, HF, and H_3PO_4 as promoters is around 64 (64.78, 64.67, and 64.38, respectively). Meanwhile, SAPO-35 in the presence of $NaNO_3$ and aqueous media SAPO-35 have shown turnover numbers of 58.52 and 57.65. The turnover frequency values were also found to be similar for SAPO-35 in the presence of $HClO_4^-$, HF, and H_3PO_4 as promoters.

This MTO reaction process will be undergoing the formation of successive construction of a C−C bond.[36] The MTO reaction is widely studied with SAPO-34 and the resulting products are mostly lower olefins like methylene and propene. In the present study, SAPO-35 was used as a catalyst, and with this catalyst, we have obtained the product with four carbons that is 2-butene. Various reaction mechanisms were proposed by different researchers,[37] from which the most studied and mentioned reaction mechanism is direct conversion mechanisms. In this reaction mechanism, the reactant methanol molecules undergo a direct coupling reaction to produce olefin products. Based on the involved reaction intermediate, there are 20 different kinds of mechanisms proposed by the earlier researchers,[37] for instance, radical species,[38] oxonium ylide,[39] carbocation,[40] and carbine.[41]

3. CONCLUSIONS

Levyne-type topological microporous SAPO-35 molecular sieves were successfully synthesized by using the conventional hydrothermal method in the presence of different inorganic promoters to reduce the reaction time in typical non-aqueous media. In the present study, the reaction time was reduced by 80%, which is highly recommended for industrial commercialization. All the materials synthesized using various promoters have exhibited similar characteristics to the standard samples (materials synthesized without using promoters), which was demonstrated using different methods in the present study. Moreover, the catalytic performance in terms of yield and selectivity of these materials in the MTO conversion reaction is found to be similar to the performance of standard materials. With the help of all these studies, it can be concluded that the addition of promoters has successfully reduced the time for the crystallization process, which in turn reduced the time for the reaction, and the materials synthesized through this method are as effective as the standard materials in the MTO conversion reaction.

4. EXPERIMENTAL SECTION

4.1. Synthesis. Aluminum isopropoxide $C_9H_{21}O_3Al$ as the Al source (98% purity, Sigma Aldrich, USA), orthophosphoric acid (H_3PO_4) as the P source (85% purity, S.D. Fine India), fumed Silica (SiO_2) as the Si source (99.8% purity, Sigma Aldrich, USA), and hexamethyleneimine ($C_6H_{12}NH$) as the structure directing agent (98% purity, Sigma Aldrich, USA) materials were used for the synthesis without any further purification.

https://dx.doi.org/10.1021/acsomega.0c06109
ACS Omega 2021, 6, 5661−5669

Table 4. Synthesis Conditions of SAPO-35

S. no.	gel composition	crystallization conditions	product
1	Al_2O_3:1.8 P_2O_5:4.9HEM:SiO_2:49EG	360 h, 200 °C	SAPO-35 (standard)
2	Al_2O_3:1.8 P_2O_5:4.9HEM:SiO_2:49EG:0.9−1.3 $HClO_4^-$	72 h, 200 °C	SAPO-35
3	Al_2O_3:1.8 P_2O_5:4.9HEM:SiO_2:49EG:1.8 $HClO_4^-$	54 h, 200 °C	semi-crystalline SAPO-35
4	Al_2O_3:1.8 P_2O_5:4.9HEM:SiO_2:49EG:1.8 $HClO_4^-$	60 h, 200 °C	semi-crystalline SAPO-35
5	Al_2O_3:1.8 P_2O_5:4.9HEM:SiO_2:49EG:0.9−1.3 $HClO_4^-$	48 h, 200 °C	amorphous
6	Al_2O_3:1.8 P_2O_5:4.9HEM:SiO_2:49EG:0.9−1.3 $NaNO_3$	168 h, 200 °C	SAPO-35
7	Al_2O_3:1.8 P_2O_5:4.9HEM:SiO_2:49EG:0.9−1.3 HF	90 h, 200 °C	SAPO-35
8	Al_2O_3:1.8 P_2O_5:4.9HEM:SiO_2:49EG:0.9−1.3 H_3PO_4	120 h, 200 °C	SAPO-35
9	Al_2O_3:1.8 P_2O_5:4.9HEM:SiO_2:49EG:0.9−1.3 NH_4Cl	168 h, 200 °C	SAPO-35 with impurity phases
10	Al_2O_3:1.8 P_2O_5:4.9HEM:SiO_2:49EG:0.9−1.3 KOH/NaOH	168 h, 200 °C	amorphous

The typical synthesis of SAPO-35 using non-aqueous media is as follows. A total of 6.05 g of aluminum isopropoxide and 45.5 g of ethylene glycol were taken into a clean beaker and mixed until the solution became homogeneous for approximately 2 h. A total of 6.024 g of H_3PO_4 was added dropwise to the above solution under constant stirring conditions. In another clean beaker, 7.27 g of hexamethyleneimine and 0.526 g of fumed silica were taken and stirred to make a homogeneous solution. Furthermore, this mixture was added to the initial gel solution and the gel ratio is Al_2O_3:1.8 P_2O_5:4.9HEM:SiO_2:49EG. For the standard SAPO-35, the above gel was transferred into a Teflon-lined 100 cm^3 stainless steel autoclave programmed at 200 °C with a ramp rate of 5 °C per minute for about 360 h. After the heat treatment, the resulting products were then centrifuged, washed with distilled water, and dried at 80 °C about overnight. The sample was further calcined at 550 °C in an ambient atmosphere for 8 h to remove the unreacted reactant species present in the framework. Here, the reaction time for crystallization was 360 h, which is very long. Therefore, to overcome this, small amounts of inorganic promoters were added to accelerate the crystallization process. For promoter-based SAPO-35 samples, after addition of fumed silica and hexamethyleneimine, appropriate amounts of promoter (Table 4) were added to the gel, which was further stirred for about 2 h and subjected to crystallization at 200 °C.

The reaction conditions and promoters used for the synthesis of SAPO-35 in a non-aqueous media are given in Table 4.

4.2. Characterization. The crystalline nature and purity of all the samples were determined by powder X-ray diffraction (PXRD) on a PANalytical X'Pert diffractometer at room temperature, with a monochromated Ni filtered Cu Kα (λ = 1.5406 Å). The X-ray scan range of 2θ was from 6 to 50°. Morphologies of the synthesized samples were analyzed using a JEOL JSM-6300 scanning electron microscope (SEM). To identify the framework structure, FT-IR spectra were recorded using a Perkin Elmer spectrometer using a KBr pellet technique in a range of 400−4000 cm^{-1}.

The solid-state magic angle spinning (MAS) nuclear magnetic resonance (NMR) spectra of the synthesized materials were acquired in a Varian spectrometer coupled with an 8.5 T wide-bore magnet. The resonant frequencies of ^{29}Si, ^{27}Al, and ^{31}P nuclei were 70.958, 93.073, and 144.593 MHz, respectively. The experiments were carried out at room temperature, with the samples filled into Zirconia rotors of 4 mm in diameter. All of the spectra were acquired using a home-built single-resonance 4 mm MAS probe. The ^{29}Si NMR spectra were obtained with a $\pi/4$ pulse width of 2 μs at a MAS frequency of 6 kHz, and a total of 12k transients were acquired with a relaxation delay of 30 s. The ^{27}Al MAS NMR spectra were acquired using a $\pi/2$ pulse width of 2 μs at a spinning rate of 7 kHz, and a sum of 10k scans were recorded with a relaxation delay of 1 s. The ^{31}P MAS NMR spectra were obtained with a $\pi/2$ pulse width of 8.5 μs at a spinning speed of 6 kHz, and a total of 1024 scans were acquired with a relaxation delay of 10 s. The ^{29}Si, ^{27}Al, and ^{31}P spectral components were referenced to tetramethylsilane (TMS) at 0 ppm, aluminum nitrate in D_2O at 0 ppm, and 85% orthophosphoric acid at 0 ppm. The data were processed using Tecmag NTNMR software.

X-ray photoelectron spectroscopic (XPS) analysis of the synthesized materials was performed using a Kratos Axis Ultra DLD spectrometer with a monochromatic Al Kα (1486.6 eV) radiation source at a power of 150 W (15 kV × 10 mA). A 3 × 3 mm area of powder sample was sputtered with an Ar ion beam (4 kV) to remove adventitious surficial carbon prior to XPS. The wide-scan survey spectra were acquired at a pass energy of 20 eV with the neutralizer turned on. Compositional analysis was conducted with CasaXPS software using a Shirley background and a Gaussian−Lorentzian peak fitting routine with standard relative sensitivity factors.

4.3. Catalytic Application Study. To know the ability of catalysts, we have performed methanol to olefin (MTO) conversion under atmospheric pressure at 350 °C. The process is as follows: 1 g of calcined SAPO-35 catalyst along with 15 g of silicon carbide was taken in a stainless steel reactor with an internal diameter of 3 cm and with a length of 60 cm. This reactor was placed in a tubular furnace and preheated to a temperature of 550 °C for 1 h in order to remove any moisture content in the catalyst. Simultaneously, the catalyst was also purged with N_2 gas with a flow rate of 150 mL/min. After the preheating process, the temperature was reduced to 350 °C, and at this temperature, the reactor was flown with a 30% methanol−water mixture with a 6.5 h^{-1} WHSV. The resulting gas products (effluent gas) were analyzed by gas chromatography (Thermo-scientific 1101) and the column used was GRS-1 dimethylpolysiloxane. The GC oven initial temperature was 40 °C, and then the temperature was ramped at 5 °C min^{-1} to 210 °C. The detector temperature was 300 °C during the analysis time. The yield percentage was calculated using eq 3

$$Y_p = \frac{\text{mg (out)} \times X_p}{m_{MeOH}} \times 100 \quad (3)$$

In eq 3, Y_p is the yield of the product in weight percentage, mg (out) is the mass flow rate of the outlet gas product, X_p is the

https://dx.doi.org/10.1021/acsomega.0c06109
ACS Omega 2021, 6, 5661−5669

mass fraction of products that were analyzed by GC, and m_{MeoH} (in) is the mass flow rate of inlet methanol.

The turnover number (TON) and turnover frequency were calculated using the following formulas:

turn over number (TON)

= number of moles of reactant converted per hour

/number of moles of active centers present in catalyst

turn over frequency (TOF)

= turn over number (TON)

/number of seconds present in hour

The turn over number and frequency represent the rate of catalysis per hour and per second.

AUTHOR INFORMATION

Corresponding Author

Venkatathri Narayanan − *Department of Chemistry, National Institute of Technology, Warangal, Telangana 506 004, India;* orcid.org/0000-0002-4586-9055; Phone: +91-9491319976; Email: venkatathrin@yahoo.com, venkatathrin@nitw.ac.in

Authors

Suresh Siliveri − *Department of Chemistry, National Institute of Technology, Warangal, Telangana 506 004, India;* orcid.org/0000-0003-2016-155X

Sai Siva Kumar Pinnepalli − *Department of Chemistry, University of Missouri-Kansas City, Kansas City, Missouri 64110-2446, United States*

Deepak Joshi − *CSIR-Indian Institute of Petroleum, Dehradun 248005, India*

Suman Chirra − *Department of Chemistry, National Institute of Technology, Warangal, Telangana 506 004, India*

Srinath Goskula − *Department of Chemistry, National Institute of Technology, Warangal, Telangana 506 004, India*

Sripal Reddy Gujjula − *Department of Chemistry, National Institute of Technology, Warangal, Telangana 506 004, India*

Nathan A. Oyler − *Department of Chemistry, University of Missouri-Kansas City, Kansas City, Missouri 64110-2446, United States*

Complete contact information is available at: https://pubs.acs.org/10.1021/acsomega.0c06109

Notes

The authors declare no competing financial interest.

ACKNOWLEDGMENTS

Authors are thankful to DST-SERB (EMR/2014/000629) Government of India for the financial support and Dr. Vimal Kumar. K (Department of Chemistry, National Institute of Technology, Warangal) for his technical support.

REFERENCES

(1) Lok, B. M.; Messina, C. A.; Patton, R. L.; Gajek, R. T.; Cannan, T. R.; Flanigen, E. M. Silicoaluminophosphate Molecular Sieves: Another New Class of Microporous Crystalline Inorganic Solids. *J. Am. Chem. Soc.* **1984**, *106*, 6092−6093.

(2) Rajic, N.; Kaucic, V.; Logar, N. Z. *Molecular Sieves: Aluminophosphates. In Encyclopedia of Catalysis*; John Wiley & Sons, Inc.: Hoboken, NJ, USA, 2011, DOI: 10.1002/0471227617.eoc151.-pub2.

(3) Qisheng, H.; Ruren, X. Syntheses of $AlPO_4$-5, $AlPO_4$-11, and $AlPO_4$-21 from Non-Aqueous Systems. *J. Chem. Soc., Chem. Commun.* **1990**, *10*, 783.

(4) Venkatathri, N.; Yoo, J. W. Synthesis, Characterization and Catalytic Properties of a LEV Type Silicoaluminophosphate Molecular Sieve, SAPO-35 from Aqueous Media Using Aluminium Isopropoxide and Hexamethyleneimine Template. *Appl. Catal., A* **2008**, *340*, 265−270.

(5) Yu, J.; Xu, R. Rich Structure Chemistry in the Aluminophosphate Family. *Acc. Chem. Res.* **2003**, *36*, 481−490.

(6) Sastre, G.; Lewis, D. W.; Catlow, C. R. A. Modeling of Silicon Substitution in SAPO-5 and SAPO-34 Molecular Sieves. *J. Phys. Chem. B* **1997**, *101*, 5249−5262.

(7) Potter, M. E. Down the Microporous Rabbit Hole of Silicoaluminophosphates: Recent Developments on Synthesis, Characterization, and Catalytic Applications. *ACS Catal.* **2020**, *10*, 9758−9789.

(8) Sastre, G.; Lewis, D. W.; Catlow, C. R. A. Mechanisms of Silicon Incorporation in Aluminophosphate Molecular Sieves. *J. Mol. Catal. A: Chem.* **1997**, *119*, 349−356.

(9) Samanta, S.; Mal, N. K.; Kumar, P.; Bhaumik, A. Hydrothermally Synthesized High Silica Mordenite as an Efficient Catalyst in Alkylation Reaction under Liquid Phase Condition. *J. Mol. Catal. A: Chem.* **2004**, *215*, 169−175.

(10) Luo, Y.; Funke, H. H.; Falconer, J. L.; Noble, R. D. Adsorption of CO_2, CH_4, C_3H_8 , and H_2O in SSZ-13, SAPO-34, and T-Type Zeolites. *Ind. Eng. Chem. Res.* **2016**, *55*, 9749−9757.

(11) Fischer, M.; Bell, R. G. Cation-Exchanged SAPO-34 for Adsorption-Based Hydrocarbon Separations: Predictions from Dispersion-Corrected DFT Calculations. *Phys. Chem. Chem. Phys.* **2014**, *16*, 21062−21072.

(12) Chen, H.; Wydra, J.; Zhang, X.; Lee, P.-S.; Wang, Z.; Fan, W.; Tsapatsis, M. Hydrothermal Synthesis of Zeolites with Three-Dimensionally Ordered Mesoporous-Imprinted Structure. *J. Am. Chem. Soc.* **2011**, *133*, 12390−12393.

(13) Suresh, S.; Reddy, I. A. K.; Venkatathri, N. Synthesis of SAPO-16 Molecular Sieve in Non-Aqueous Medium by Microwave Method Using Hexamethyleneimine as a Template. *Microporous Mesoporous Mater.* **2018**, *263*, 275−281.

(14) Zheng, C.; Li, Y.; Yu, J. Database of Open-Framework Aluminophosphate Structures. *Sci. Data* **2020**, *7*, 107.

(15) Meng, X.; Xiao, F.-S. Green Routes for Synthesis of Zeolites. *Chem. Rev.* **2014**, *114*, 1521−1543.

(16) Meng, X.; Wang, L.; Xiao, F.-S. Sustainable Routes for Synthesis of Zeolite Catalysts. In *Nanotechnology in Catalysis*; Wiley-VCH Verlag GmbH & Co. KGaA: Weinheim, Germany, 2017; pp. 251−274, DOI: 10.1002/9783527699827.ch11.

(17) Kumar, R.; Bhaumik, A.; Ahedi, R. K.; Ganapathy, S. Promoter-Induced Enhancement of the Crystallization Rate of Zeolites and Related Molecular Sieves. *Nature* **1996**, *381*, 298−300.

(18) Siliveri, S.; Chirra, S.; Tyagi, C.; Gandamalla, A.; Adepu, A. K.; Goskula, S.; Gujjula, S. R.; Venkatathri, N. New Porous High Surface Area, TiO_2 Anatase/SAPO-35 Mild Brønsted Acidic Nanocomposite: Synthesis, Characterization and Studies on It's Enhanced Photocatalytic Activity. *ChemistrySelect* **2019**, *4*, 9135−9142.

(19) Lohse, U.; Vogt, F.; Richter-Mendau, J. Synthesis and Characterization of the Levyne-like Structure SAPO-35, Prepared with Cyclohexylamine as Templating Agent. *Cryst. Res. Technol.* **1993**, *28*, 1101−1107.

(20) Venkatathri, N.; Hegde, S. G.; Rajamohanan, P. R.; Sivasanker, S. Synthesis of SAPO-35 in Non-Aqueous Gels. *J. Chem. Soc., Faraday Trans.* **1997**, *93*, 3411−3415.

(21) Tian, P.; Wei, Y.; Ye, M.; Liu, Z. Methanol to Olefins (MTO): From Fundamentals to Commercialization. *ACS Catal.* **2015**, *5*, 1922−1938.

(22) Wang, Q.; Wang, L.; Wang, H.; Li, Z.; Wu, H.; Li, G.; Zhang, X.; Zhang, S. Synthesis, Characterization and Catalytic Performance

of SAPO-34 Molecular Sieves for Methanol-to-Olefin (MTO) Reaction. *Asia-Pacific J. Chem. Eng.* **2011**, *6*, 596−605.
(23) Dai, W.; Wu, G.; Li, L.; Guan, N.; Hunger, M. Mechanisms of the Deactivation of SAPO-34 Materials with Different Crystal Sizes Applied as MTO Catalysts. *ACS Catal.* **2013**, *3*, 588−596.
(24) Yarulina, I.; Chowdhury, A. D.; Meirer, F.; Weckhuysen, B. M.; Gascon, J. Recent Trends and Fundamental Insights in the Methanol-to-Hydrocarbons Process. *Nat. Catal.* **2018**, *1*, 398−411.
(25) Wang, Y.; Chen, S.-L.; Gao, Y.-L.; Cao, Y.-Q.; Zhang, Q.; Chang, W.-K.; Benziger, J. B. Enhanced Methanol to Olefin Catalysis by Physical Mixtures of SAPO-34 Molecular Sieve and MgO. *ACS Catal.* **2017**, *7*, 5572−5584.
(26) Ahn, N. H.; Seo, S.; Hong, S. B. Small-Pore Molecular Sieves SAPO-57 and SAPO-59: Synthesis, Characterization, and Catalytic Properties in Methanol-to-Olefins Conversion. *Catal. Sci. Technol.* **2016**, *6*, 2725−2734.
(27) Venkatathri, N.; Hegde, S. G. United States Patent: US 7,037,874 B2, 2006, US007037874B2.
(28) Klinowski, J. Solid-State NMR Studies of Molecular Sieve Catalysts. *Chem. Rev.* **1991**, *91*, 1459−1479.
(29) Klinowski, J.; Anderson, M. W. Solid-State NMR Studies of the Structure and Reactivity of Molecular Sieve Catalysts. *Magn. Reson. Chem.* **1990**, *28*, S68−S81.
(30) Tian, P.; Li, B.; Xu, S.; Su, X.; Wang, D.; Zhang, L.; Fan, D.; Qi, Y.; Liu, Z. Investigation of the Crystallization Process of SAPO-35 and Si Distribution in the Crystals. *J. Phys. Chem. C* **2013**, *117*, 4048−4056.
(31) Jung, H. J.; Shin, C.-H.; Hong, S. B. Si Distribution in Silicoaluminophosphate Molecular Sieves with the LEV Topology: A Solid-State NMR Study. *J. Phys. Chem. B* **2005**, *109*, 20847−20853.
(32) Zhang, L.; Huang, Y. New Insights into Formation of Molecular Sieve SAPO-34 for MTO Reactions. *J. Phys. Chem. C* **2016**, *120*, 25945−25957.
(33) Xu, L.; Du, A.; Wei, Y.; Wang, Y.; Yu, Z.; He, Y.; Zhang, X.; Liu, Z. Synthesis of SAPO-34 with Only Si(4Al) Species: Effect of Si Contents on Si Incorporation Mechanism and Si Coordination Environment of SAPO-34. *Microporous Mesoporous Mater.* **2008**, *115*, 332−337.
(34) Vomscheid, R.; Briend, M.; Peltre, M. J.; Man, P. P.; Barthomeuf, D. The Role of the Template in Directing the Si Distribution in SAPO Zeolites. *J. Phys. Chem.* **1994**, *98*, 9614−9618.
(35) Kumar, R.; Mukherjee, P.; Pandey, R. K.; Rajmohanan, P.; Bhaumik, A. Role of Oxyanions as Promoter for Enhancing Nucleation and Crystallization in the Synthesis of MFI-Type Microporous Materials. *Microporous Mesoporous Mater.* **1998**, *22*, 23−31.
(36) Yarulina, I.; Chowdhury, A. D.; Meirer, F.; Weckhuysen, B. M.; Gascon, J. Recent trends and fundamental insights in the methanol-to-hydrocarbons process. *Nat. Catal.* **2018**, *1*, 398−411.
(37) Stöcker, M. Methanol-to-Hydrocarbons: Catalytic Materials and Their Behavior. *Microporous Mesoporous Mater.* **1999**, *29*, 3−48.
(38) Clarke, J. K. A.; Darcy, R.; Hegarty, B. F.; O'Donoghue, E.; Amir-Ebrahimi, V.; Rooney, J. J. Free Radicals in Dimethyl Ether on H-ZSM-5 Zeolite. A Novel Dimension of Heterogeneous Catalysis. *J. Chem. Soc., Chem. Commun.* **1986**, *5*, 425.
(39) Hutchings, G. J.; Gottschalk, F.; Hall, M. V. M.; Hunter, R. Hydrocarbon Formation from Methylating Agents over the Zeolite Catalyst ZSM-5. Comments on the Mechanism of Carbon−Carbon Bond and Methane Formation. *J. Chem. Soc., Faraday Trans. 1* **1987**, *83*, 571.
(40) Ono, Y.; Mori, T. Mechanism of Methanol Conversion into Hydrocarbons over ZSM-5 Zeolite. *J. Chem. Soc., Faraday Trans. 1* **1981**, *77*, 2209.
(41) Chang, C. D.; Silvestri, A. J. The Conversion of Methanol and Other O-Compounds to Hydrocarbons over Zeolite Catalysts. *J. Catal.* **1977**, *47*, 249−259.

https://dx.doi.org/10.1021/acsomega.0c06109
ACS Omega 2021, 6, 5661−5669